AIP | Applied Physics Letters

Transparent organic thin film transistors with WO3/Ag/WO3 source-drain electrodes fabricated by thermal evaporation

Nan Zhang, Yongsheng Hu, and Xingyuan Liu

Citation: Applied Physics Letters **103**, 033301 (2013); doi: 10.1063/1.4813838
View online: http://dx.doi.org/10.1063/1.4813838
View Table of Contents: http://scitation.aip.org/content/aip/journal/apl/103/3?ver=pdfcov
Published by the AIP Publishing

Transparent organic thin film transistors with WO_3/Ag/WO_3 source-drain electrodes fabricated by thermal evaporation

Nan Zhang,[1,2] Yongsheng Hu,[1,2] and Xingyuan Liu[1,a)]
[1]*State Key Laboratory of Luminescence and Applications, Changchun Institute of Optics, Fine Mechanics and Physics, Chinese Academy of Sciences, Changchun 130033, China*
[2]*Graduate University of Chinese Academy of Sciences, Beijing 130039, China*

(Received 19 February 2013; accepted 28 June 2013; published online 15 July 2013)

High-performance transparent organic thin film transistors using a WO_3/Ag/WO_3 (WAW) multilayer as the source and drain electrodes have been developed without breaking the vacuum. The WAW electrodes were deposited by thermal evaporation at room temperature, leading to little damage to organic film. The optimized WAW electrode shows high transmittance (86.57%), low sheet resistance (11 Ω/sq), and a high work function (5.0 eV). Consequently, we obtained high performance devices with mobility of 8.44×10^{-2} $cm^2/V \cdot s$, an on/off ratio of approximately 1.2×10^6, and an average visible range transmittance of 81.5%. © *2013 AIP Publishing LLC*. [http://dx.doi.org/10.1063/1.4813838]

In the past few decades, great progress has been made in the development of organic thin film transistors (OTFTs) and they are receiving increasing attention because of their potential applications, including displays, e-papers, sensors, and radio frequency identification tags. Previous studies have demonstrated that the field-effect mobility of OTFTs was not only comparable but actually superior to that of a-Si TFTs.[1] Recently, there have been increased research efforts to develop transparent OTFTs, which are one of the most promising pixel driving components for transparent active matrix displays, such as liquid crystal displays or organic light emitting devices (OLEDs). While, shift phenomenon in electrical characteristics when exposed OTFTs to illumination need further studies in order to be used in displays.[2–4] Thus far, for transparent OTFTs, various transparent conductive films, including indium tin oxide (ITO),[5] Al:ZnO (AZO),[6] NiO_x,[7] carbon nanotube,[8] graphene,[9] and reduced graphene oxide[10] have been used as source-drain (S/D) electrodes. However, they suffer from low work function,[5,6] high substrate temperature,[5,6] low transmittance[7] and high sheet resistance,[8–10] which cause increased contact resistance,[5,6] non-uniform organic semiconductor film,[6,8,9] reduced device transmittance,[7] sputter damage to the organic active layer,[11–14] and a severe negative impact on the performance of transparent OTFTs. Sputter damage can also be found in OLEDs.[15,16] In addition, a proper energy matching with organic semiconductor of these transparent conductive films is the issue that needs to be resolved. To date, fabrication process and properties of transparent conductive films as the S/D electrodes of OTFTs have been far from satisfactory.

According to previous studies, when a metal layer with high reflection is inserted between two dielectric layers with high refractive indexes, this dielectric-metal-dielectric (DMD) structure can achieve an enhanced transmittance in a selective region through the interference effect.[17–19] The multilayer transparent films based on a DMD structure can be optimized by tuning the thicknesses of the dielectric and metal layers to obtain high conductivity and high transparency in the visible region.[20,21] In this letter, we have developed high-performance transparent OTFTs based on transparent source and drain electrodes with a DMD structure of WO_3/Ag/WO_3 (WAW). The WAW electrodes were deposited by thermal evaporation at room temperature without causing sputter damage to the active layer, and the devices were fabricated without breaking the vacuum. WAW electrodes deposited on glass substrates show excellent electrical and optical properties, which are comparable to those of ITO electrodes. Also, the WAW structure can be patterned by using lithographic masking methods, and its higher work function means good energy matching with the energy level of the highest occupied molecular orbital (HOMO) of the organic materials. Transparent pentacene OTFTs with WAW electrodes have demonstrated good device performance, including a field-effect mobility of 8.44×10^{-2} $cm^2/V \cdot s$, an on/off ratio of approximately 1.2×10^6, and a visible range transmittance of 81.5%.

The WAW transparent electrodes were deposited on ultrasonically cleaned (with acetone, ethanol, and de-ionized water) glass substrates. The WO_3 was fully degassed in vacuum for 1 h prior to the deposition process. WO_3 (25 nm), Ag (9 nm), and WO_3 (25 nm) films were prepared under a vacuum pressure of 1.8×10^{-4} Pa and were thermally evaporated sequentially at room temperature. The evaporation rates of WO_3 and Ag were 0.1 nm/s and 1 nm/s, respectively. Pentacene and poly(methyl methacrylate) (PMMA, $M_W = 996\,000$) were purchased from Aldrich and were used without further treatment. The ITO electrodes were deposited by RF magnetron sputtering at room temperature. The ITO gate electrodes were patterned by photolithography and wet etching. The ITO glass substrates were then ultrasonically cleaned with acetone, ethanol, and deionized water in sequence. After that, PMMA, serving as an organic dielectric layer, was prepared from 8 wt. % PMMA in toluene. The PMMA layer was annealed at 80 °C for 6 h in a glove-box. The thickness of the PMMA layer was 350 nm. Next, 40 nm-thick pentacene was deposited and patterned on the PMMA layer with a shadow mask by thermal evaporation at room temperature. The evaporation rate of pentacene was 0.1 nm/s

a)Electronic mail: liuxy@ciomp.ac.cn

under a vacuum of 1.6×10^{-4} Pa. Finally, the sample was transferred to another chamber without breaking the vacuum, and then the WAW source and drain electrodes were deposited on the pentacene layer through a shadow mask. The channel length and width are 75 μm and 3 mm, respectively. A quartz-crystal oscillator placed near the substrate is used to monitor the thickness and deposition rate of the thin film transistors, which is calibrated *ex situ* using a surface profiler (Ambios XP-1). Optical transmittance spectra were measured with a Shimadzu UV-3101PC spectrophotometer. The sheet resistance was measured using the four-point probe method with a surface resistivity meter. The work function of WAW and ITO was measured by a KP Technology Ambient Kelvin probe system package. The electrical characteristics, including the voltage–current and capacitance measurements, are determined with Keithley 4200 SCS at room temperature under air ambient.

To optimize the optical transmittance of the WAW electrodes, we have calculated the transmittance of the WAW structures at 550 nm as a function of the WO_3 and Ag layer thicknesses. Figure 1(a) shows that the transmittance of WAW can be optimized to over 90% and the good transmittance values are achieved with WO_3 layer thicknesses from 20 to 50 nm, and Ag layer thicknesses from 8 to 16 nm. Our calculations also show that the average visible range transmittance ($\lambda = 400$–750 nm) of WAW can be enhanced up to 91.6% by fixing the Ag thickness at 9 nm and varying the thicknesses of both WO_3 layers (Fig. 1(b)). The measured transmittance spectra of WAW and ITO films are shown in Fig. 1(c) for comparison. The average transmittance of the WAW film is 86.57% over the 400–750 nm range, which is very close to that of ITO (86.65%). Sheet resistance is also an important parameter of transparent conductive films. Figure 1(d) shows the change in the measured sheet resistance and transmittance ($\lambda = 550$ nm) of WAW electrodes as a function of the Ag thickness. The WAW sheet resistance decreases dramatically from 40 Ω/sq to 5 Ω/sq with increasing Ag thickness. With the thickness of Ag layer increased to above 8 nm, the sheet resistance value of WAW film is very low, which shows that the Ag layer has formed a continuous film.[22,23] The WAW structure shows greater transparency at Ag thicknesses in the 8–12 nm range, especially for the 9 nm-thick sample at 90.1%. At Ag thickness of below 8 nm and above 15 nm, the lower transmittance values result from the discontinuous growth of Ag and the high reflectance of Ag layer, respectively.[24,25] From the simulation and experimental data, we can confirm that the WAW structure (layer thickness of 25/9/25 nm, average transmittance of 86.57%, and sheet resistance of 11 Ω/sq) has competitive properties in comparison with other transparent electrode materials.

We fabricated pentacene OTFTs with WAW and ITO source-drain electrodes, respectively. ITO was deposited through the shadow masks at room temperature by RF sputtering. In order to compare the device performance, the thickness of the ITO films was also limited to 59 nm. The measured sheet resistivity of the ITO was 80 Ω/sq. We found that transparent OTFTs cannot be realized with ITO S/D electrodes. The measured results of the devices did not show typical output and transfer characteristics of OTFTs. We measured the transmittance spectra of glass/ITO/PMMA/pentacene stacks with and without a 59-nm-thick ITO film on top. In the Fig. 2(a), the absorption peak observed near 670 nm is related to the orbital gap (1.8 eV) of pentacene between the HOMO and the lowest unoccupied molecular orbital (LUMO), and the other spectral features correspond to the other unoccupied energy levels of pentacene.[7,26] However, when the ITO S/D electrodes were deposited on the pentacene, the absorption peaks of pentacene disappeared. To further confirm the *sputter damage* effect of ITO deposition process on the pentacene layer, we also measured the photoluminescence spectra of the ITO glass substrate, the device with and without ITO S/D electrodes (Fig. 2(b)). The spectrum features between 625 nm to 700 nm (indentified by the red arrowhead) are related to the pentacene

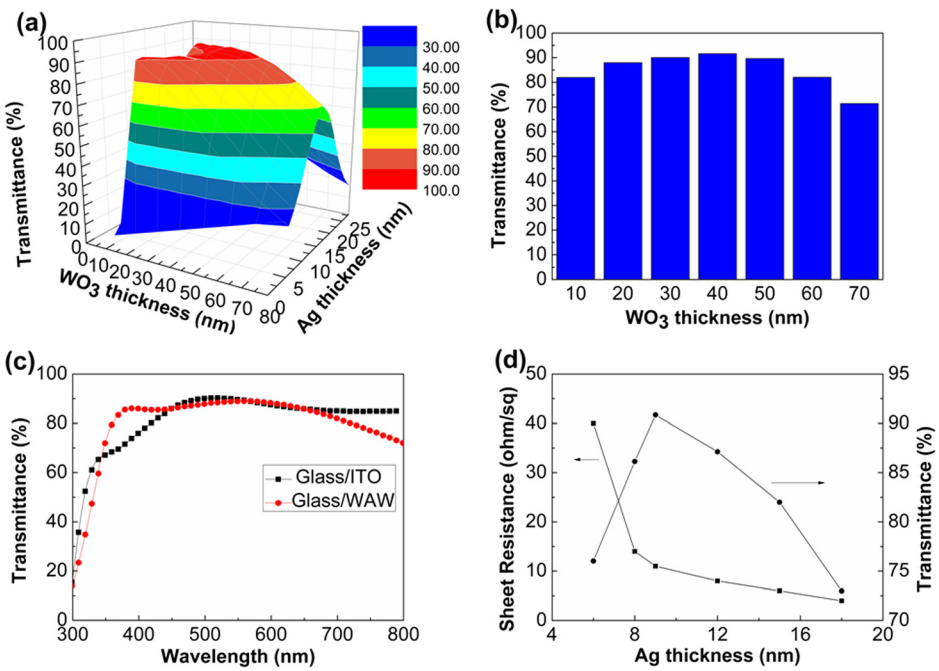

FIG. 1. (a) Calculated transmittance of the WAW structure at a wavelength of 550 nm as a function of WO_3 and Ag thicknesses. (b) Calculated visible range average transmittance of the WAW films with different WO_3 layer thicknesses. The Ag thickness is fixed at 9 nm. (c) Transmittance spectra of ITO and WAW. (d) Transmittance at a wavelength of 550 nm and the sheet resistance of the WAW electrodes as a function of Ag thickness. The WO_3 thickness is fixed at 25 nm.

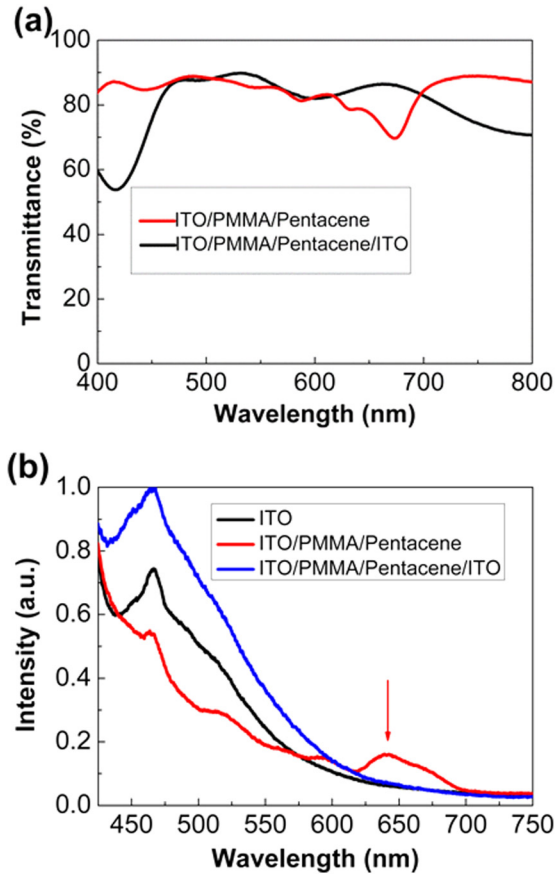

FIG. 2. (a) Transmittance spectra of the 40 nm-thick pentacene/350 nm-thick PMMA/ITO glass structure with and without the ITO electrode structure on top. (b) Photoluminescence spectra of the ITO glass substrate, the OTFTs with and without ITO source-drain electrodes excited at 400 nm.

films,[27,28] and other most features in the spectra are from the ITO film (especially indium oxide).[29,30] The emission from pentacene film cannot be observed in the OTFT with the ITO S/D electrodes, which implies that ITO sputtering deposition process has a strong negative effect on the underlying organic layer,[12,13] and energetic ion sputter damage should be the major reason of device failures. Although there were some methods to protect the organic layer from sputtering damage,[13,31] we cannot find any experimental details in the transparent OTFTs.

Figures 3(a) and 3(b) show the typical output and transfer characteristics of the transparent OTFTs with WAW S/D electrodes, and the inset of Fig. 3(a) shows the device structure. The output characteristic curves in Fig. 3(a) show that the transparent OTFTs operate in an accumulation mode using a negative bias to the gate electrode, because the concentration of the majority carriers produces an increase in I_D,[5] and that the linear and saturation regimes have a clear gate-voltage dependence.[9] The field-effect mobility of the devices is obtained from the following equation:

$$I_D = \mu C_i (W/2L)(V_G - V_T)^2, \quad (1)$$

where I_D, C_i, μ, V_G, V_T, W, and L are the drain current, the capacitance per unit area of the gate dielectric, the mobility, the gate voltage, the threshold voltage, the channel width, and the channel length, respectively. The dielectric constant

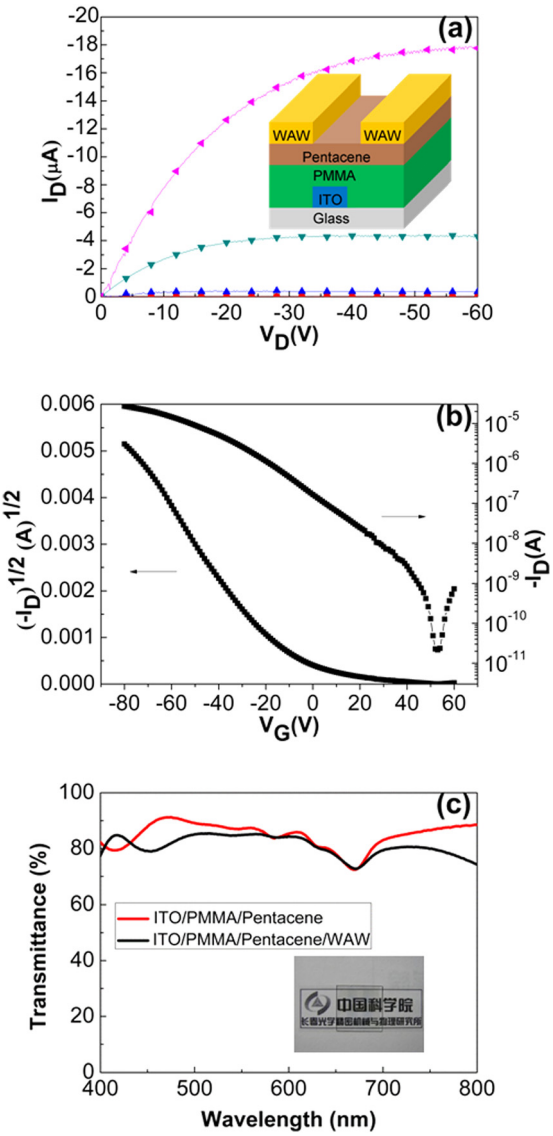

FIG. 3. (a) Output characteristic curves. Inset: a schematic of the OTFT structure with WAW S/D electrodes. (b) Transfer characteristic curves of the OTFT with WAW S/D electrodes at $V_D = -30$ V. (c) The transmittance spectra of the 40 nm-thick pentacene/350 nm-thick PMMA/ITO glass structure with and without the WAW electrode structure on top. Inset: a photo of a 4-device array of these transparent OTFTs positioned above a CIOMP logo.

(ε_r) is measured as being approximately 3.0, which agrees with the results of a previous report.[32] Therefore, C_i can be calculated to be about 7.6 nF/cm^2 and the derived μ value is 8.44×10^{-2} cm^2/V · s, which is comparable to that of OTFTs with a PMMA dielectric layer and a pentacene active layer.[33] Also, the transfer characteristics in Fig. 3(b) show a low off-current of 2.05×10^{-11} A and a high on/off ratio of approximately 1.2×10^6. As shown in Fig. 3(c), the OTFT with the WAW S/D electrodes shows an average transmittance (400–800 nm) of 81.5%, which is very close to the transmittance of 84.3% achieved in pentacene/PMMA/ITO glass stacks in the visible range (from 400 nm to 750 nm). The absorption peak of pentacene film can also be observed near 670 nm in the spectra.[7,26] This indicates that high performance transparent OTFTs can be realized by using the WAW electrodes with negligible damage to the pentacene layer during the electrode deposition process. The inset of

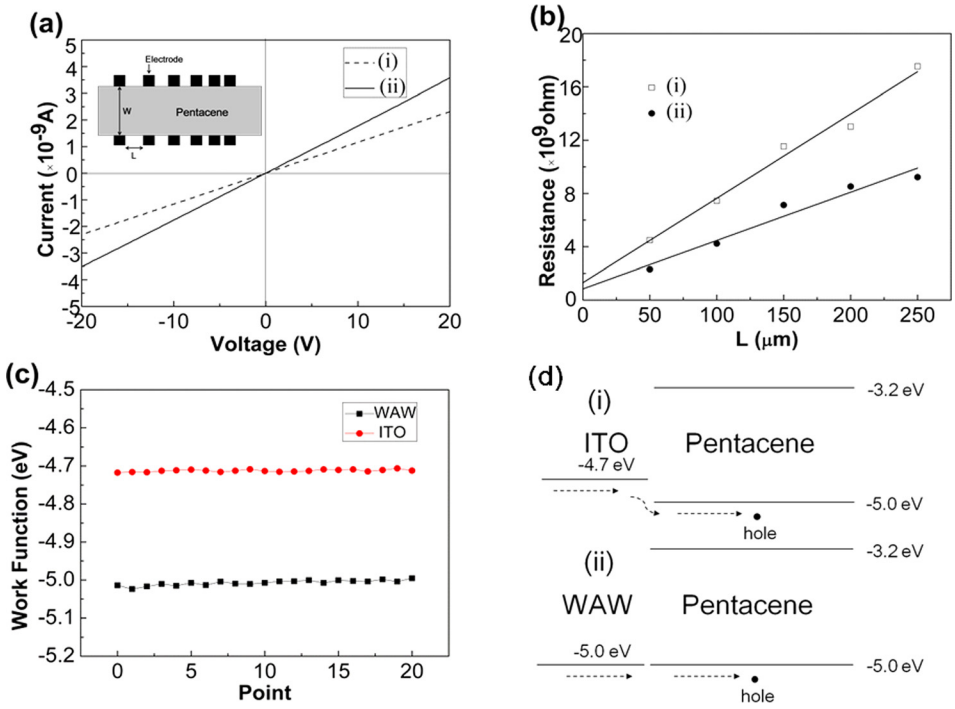

FIG. 4. (a) I-V curves for (i) ITO/pentacene and (ii) WAW/pentacene samples. Inset: the sample structure. (b) TLM-estimated data of the (i) ITO/pentacene and (ii) WAW/pentacene samples. (c) Work functions of ITO and WAW. (d) The energy diagrams at the (i) ITO/pentacene and (ii) WAW/pentacene interfaces.

Fig. 3(c) shows the photo of a 4-device array of transparent OTFTs positioned above a CIOMP logo.

Apart from the optical-electrical characteristics of transparent conductive films and device fabrication process, the interface contact resistance between the transparent electrodes and the organic semiconductors is also an important factor that dominates the performance of transparent OTFTs. The contact resistance of WAW/pentacene has been compared with the ITO/pentacene structure in which pentacene films were deposited on top of the transparent electrodes. To quantify the contact resistance between the transparent electrode materials and the pentacene semiconductor, we measured the I-V curves and transmission line method (TLM) data (Figs. 4(a) and 4(b)) of the structures. The total resistance (R_T) as a function of the distance L is given by

$$R_T = R_S L/W + 2R_C, \tag{2}$$

where R_T is the total resistance between two contacts, R_C is the contact resistance, R_S is the sheet resistance of the pentacene layer, L is the channel length, and W is the contact electrode width. The linear I-V behavior shown in Fig. 4(a) ($L = 100\,\mu m$, $W = 3$ mm) indicates that the R_T of the WAW/pentacene structure is lower than that of the ITO/pentacene structure. Fig. 4(b) shows a plot of R_C as a function of channel length L. R_C can be obtained from the intercepts of linear fits to the data. The R_C values of the ITO/pentacene and WAW/pentacene structures are $1.3 \times 10^9\ \Omega$ and $8.4 \times 10^8\ \Omega$, respectively. In addition, since WO_3 is a hole transport material[34,35] and the Fermi level of WO_3 ranges from 4.50 to 6.00 eV,[25,36,37] WAW shows a higher work function (5.0 eV) than ITO (4.7 eV) (Fig. 4(c)). Based on the results shown in Figs. 4(a) and 4(b), we find that the I-V curve of the WAW/pentacene structure is better than that of the ITO/pentacene structure, and that the R_C of WAW/pentacene is lower than that of ITO/pentacene. These results suggest that better contact is formed at the WAW/pentacene interface with a lower energy barrier. Fig. 4(d) indicates that the hole injection barrier at the pentacene/ITO interface is approximately 0.3 eV, while this energy barrier is negligible at the pentacene/WAW interface. This suggests that holes would be injected from the WAW electrode to pentacene or output from pentacene to the WAW electrode more readily.[13] This corresponds with the difference in contact resistance shown in Fig. 4(b). Lee *et al.* reported that the work function of an ITO electrode can be increased by treating the ITO electrode with ozone or oxygen (O_2) plasma, and they suggested that this higher work function might lower the energy barrier and enhance hole injection, thus producing remarkable increases in the field-effect mobility.[38] An indium cerium oxide (ICO) transparent conductor was developed by Chu *et al.*[39] They found that the lower contact resistivity of the ICO/pentacene sample in comparison with the ITO/pentacene sample might be attributed to ICO having a higher surface work function than ITO. On the other hand, some organic and inorganic materials layers were also inserted between pentacene and the transparent source/drain electrodes as buffer layers to increase the work function and reduce the hole injection barrier.[13,14] These layers could also result in the decreased contact resistance and improved device performance. Therefore, compared with ITO, the WAW S/D electrodes have high transmittance, high work function, low sheet resistance, and a deposition process under room temperature without causing damage to the active layer, which contribute to high transmittance of the device, good energy matching and low contact resistance at the organic/electrode interface, and show greater potential for achieving high performance transparent OTFTs.

In summary, high performance pentacene-based transparent OTFTs using WO_3/Ag/WO_3 layers for the source and drain electrodes have been developed. The WAW electrodes, which were grown by vacuum evaporation at room temperature, have high average transmittance of 86%, low sheet

resistance of 11 Ω/sq, and a work function of 5.0 eV. The devices were fabricated without sputtering damage and breaking the vacuum. We have demonstrated that these transparent OTFTs have good field-effect mobility of 8.44×10^{-2} $cm^2/V \cdot s$, a high on/off ratio of approximately 1.2×10^6, and an average visible range transmittance of 81.5%. These results indicate that the DMD structure is an excellent choice for the transparent electrode that will afford more opportunities to develop high performance transparent OTFTs. The applications of WAW in flexible and transparent ambipolar OTFTs will be subject to further study.

The authors acknowledge financial support by the CAS Innovation Program, the Jilin Province Science and Technology Research Project No. 20090346, and National Science Foundation of China, Nos. 51102228, 51103144, and 61106057.

[1]C. H. Wang, C. Y. Hsieh, and J. C. Hwang, Adv. Mater. **23**, 1630 (2011).
[2]Y. Zhao, G. Dong, L. Wang, and Y. Qiu, Appl. Phys. Lett. **90**, 252110 (2007).
[3]C. S. Suchand Sangeeth, P. Stadler, S. Schaur, N. S. Sariciftci, and Reghu Menon, J. Appl. Phys. **108**, 113703 (2010).
[4]C. Chuang, S. T. Tsai, Y. S. Lin, F. C. Chen, and H. D. Shieh, Jpn. J. Appl. Phys. Part 1 **46**, L1197 (2007).
[5]H. Ohta, T. Kambayashi, K. Nomura, M. Hirano, K. Ishikawa, H. Takezoe, and H. Hosono, Adv. Mater. **16**, 312 (2004).
[6]D. J. Yun and S. W. Rhee, Thin Solid Films **517**, 4644 (2009).
[7]J. M. Choi, D. K. Hwang, J. H. Kim, and S. Im, Appl. Phys. Lett. **86**, 123505 (2005).
[8]Q. Cao, Z. T. Zhu, M. G. Lemaitre, M. G. Xia, M. Shim, and J. A. Rogers, Appl. Phys. Lett. **88**, 113511 (2006).
[9]W. H. Lee, J. Park, S. H. Sim, S. B. Jo, K. S. Kim, B. H. Hong, and K. Cho, Adv. Mater. **23**, 1752 (2011).
[10]K. Suganuma, S. Watanabe, T. Gotou, and K. Ueno, Appl. Phys. Express **4**, 021603 (2011).
[11]Y. S. Park and H. K. Kim, Thin Solid Films **519**, 8018 (2011).
[12]Y. J. Lin, Y. C. Li, T. C. Wen, L. M. Huang, Y. K. Chen, H. J. Yeh, and Y. H. Wang, Appl. Phys. Lett. **93**, 043305 (2008).
[13]Y. C. Li, Y. J. Lin, C. Y. Wei, Z. X. Lin, T. C. Wen, M. Y. Chang, C. L. Tsai, and Y. H. Wang, Appl. Phys. Lett. **95**, 163303 (2009).
[14]S. J. Kim, J. M. Song, and J. S. Lee, J. Mater. Chem. **21**, 14516 (2011).
[15]L. S. Hung, L. S. Liao, C. S. Lee, and S. T. Lee, J. Appl. Phys. **86**, 4607 (1999).
[16]L. S. Hung and C. W. Tang, Appl. Phys. Lett. **74**, 3209 (1999).
[17]T. Winkler, H. Schmidt, H. Flügge, F. Nikolayzik, I. Baumann, S. Schmale, T. Weimann, P. Hinze, H.-H. Johannes, T. Rabe, S. Hamwi, T. Riedl, and W. Kowalsky, Org. Electron. **12**, 1612 (2011).
[18]Y. S. Park, H. K. Park, J. A. Jeong, H. K. Kim, K. H. Choi, S. I. Na, and D. Y. Kimc, J. Electrochem. Soc. **156**, H588 (2009).
[19]Y. Y. Choi, K.-H. Choi, H. Lee, H. Lee, J. W. Kang, and H.-K. Kim, Sol. Energy Mater. Sol. Cells **95**, 1615 (2011).
[20]C. Y. Song, H. Chen, Y. Fan, J. Luo, X. Y. Guo, and X. Y. Liu, Appl. Phys. Express **5**, 041102 (2012).
[21]X. Y. Guo, J. Lin, H. Chen, X. Zhang, Y. Fan, J. Luo, and X. J. Liu, J. Mater. Chem. **22**, 17176 (2012).
[22]X. Liu, X. Cai, J. Qiao, J. Mao, and N. Jiang, Thin Solid Films **441**, 200 (2003).
[23]H. Hoffmann and J. Vancea, Thin Solid Films **85**, 147 (1981).
[24]A. Indluru and T. L. Alford, J. Appl. Phys. **105**, 123528 (2009).
[25]K. Hong, K. Kim, S. Kim, I. Lee, H. Cho, S. Yoo, H. W. Choi, N. Y. Lee, Y. H. Tak, and J. L. Lee, J. Phys. Chem. C **115**, 3453 (2011).
[26]S. S. Kim, Y. S. Choi, K. Kim, J. H. Kim, and S. Im, Appl. Phys. Lett. **82**, 639 (2003).
[27]R. He, N. G. Tassi, G. B. Blanchet, and A. Pinczuk, Appl. Phys. Lett. **96**, 263303 (2010).
[28]S. P. Park, S. S. Kim, J. H. Kim, C. N. Whang, and S. Im, Appl. Phys. Lett. **80**(16), 2872 (2002).
[29]X. Teng, H. Fan, S. Pan, C. Ye, and G. Li, Mater. Lett. **61**, 201 (2007).
[30]S. Kaleemulla, A. Sivasankar Reddy, S. Uthanna, and P. Sreedhara Reddy, J. Alloys Compd. **479**, 589 (2009).
[31]H. K. Kim, D. G. Kim, K. S. Lee, M. S. Huh, S. H. Jeong, K. I. Kim, and T. Y. Seong, Appl. Phys. Lett. **86**, 183503 (2005).
[32]J. Zhou and F. Zhang, Appl. Phys. Lett. **91**, 253507 (2007).
[33]J. A. Cheng, C. S. Chuang, M. N. Chang, Y. C. Tsai, H. Pi, and D. Shieh, Org. Electron. **9**, 1069 (2008).
[34]C. Tao, S. Ruan, G. Xie, X. Kong, L. Shen, F. Meng, C. Liu, X. Zhang, W. Dong, and W. Chen, Appl. Phys. Lett. **94**, 043311 (2009).
[35]S. Han, W. S. Shin, M. Seo, D. Gupta, S. J. Moon, and S. Yoo, Org. Electron. **10**, 791 (2009).
[36]C. Bechinger, S. Herminghaus, and P. Leiderer, Thin Solid Films **239**, 156 (1994).
[37]M. J. Son, S. Kim, S. Kwon, and J. W. Kim, Org. Electron. **10**, 637 (2009).
[38]H. S. Lee, J. H. Cho, W. K. Kim, J. L. Lee, and K. Cho, Electrochem. Solid-State Lett. **10**, H239 (2007).
[39]J. A. Chu, J. J. Zeng, K. C. Wu, and Y. J. Lin, Thin Solid Films **519**, 868 (2010).